

Local Advective Mechanism for Interdecadal Variability in Circulations Driven by Constant Surface Heat Fluxes in Idealized Basins

YOUNG-GYU PARK^{1*} and JIN HWAN HWANG²

¹*Ocean Climate Change and Coastal Disaster Research Department, Korea Ocean Research and Development Institute, Sa-dong, Ansan 426-744, Korea*

²*Department of Civil and Environmental System Engineering, Dongguk University, Pil-dong, Chung-gu, Seoul 100-715, Korea*

(Received 14 July 2008; in revised form 27 April 2009; accepted 30 April 2009)

Idealized numerical experiments with a depth level coordinate ocean circulation model (GFDL MOM3) have been conducted to investigate the structure of interdecadal variability from thermally driven circulations. The model oceans are driven by steady surface heat fluxes in the absence of surface wind stresses. Interdecadal variability is observed, with characteristics similar to those reported in many previous studies. To explain the nature of the variability we propose a new mechanism based on two local horizontal advective processes. This overcomes the limitations in previous theories based on the interplay between global properties such as zonal and meridional temperature gradients and overturning. One of the two advective processes is a zonal flow anomaly induced by a temperature anomaly along the northern wall through geostrophy southward of the temperature anomaly. A cold (warm) anomaly along the northern wall produces a positive (negative) zonal flow anomaly that induces a warm (cold) temperature anomaly by enhancing (weakening) warm advection from the western boundary along the path of the zonal flow anomaly. The temperature and flow anomalies are transported toward the eastern boundary by the mean eastward zonal flow. When the positive (negative) zonal flow anomaly that accompanies the warm (cold) temperature anomaly encounters the eastern wall, a downwelling (upwelling) anomaly is produced. To dissipate the vorticity due to this downwelling (upwelling) anomaly, a northward (southward) flow anomaly, which is another advective process governing the variability, is generated within a frictional boundary layer next to the eastern wall. The northward (southward) flow anomaly circulates cyclonically along the perimeter of the basin while enhancing (reducing) warm advection. So does the warm (cold) temperature anomaly carried to the eastern wall by the mean zonal flow while pushing the cold (warm) anomaly that produced the positive (negative) zonal flow anomaly westward and initiating the other half cycle of the variability. During the anomalous downwelling or upwelling, the available potential energy stored in the anomalous density field is released to maintain the variability. Thus, neither barotropic nor baroclinic instability supplies energy for the variability. The anomalous vertical velocity is stronger along the northern boundary and the northern part of the eastern boundary. A shallow continental slope added along those boundaries prohibits the anomalous vertical motion and weakens variability very effectively, while one along the western boundary does not.

Keywords:

- Thermohaline variability,
- interdecadal variability,
- ocean modeling.

1. Introduction

To reduce the thermal gradient between the equator and poles, the oceanic thermohaline circulation (THC, hereafter) transports a substantial part of the solar energy accumulated in the tropical oceans to high latitude oceans

* Corresponding author. E-mail: ypark@kordi.re.kr

(Vonder Haar and Oort, 1973; Trenberth and Caron, 2001; Trenberth *et al.*, 2001; Wunsch, 2005). Thus THC is an important component of the earth's climate system, and its diverse aspects have been studied quite extensively through observational (Clarke *et al.*, 2001), theoretical or numerical methods, ranging from simple idealistic models to realistic ones (see Dijkstra (2000) for review). Among various aspects of THC, its interdecadal variability has been studied in many ways, since the variability could be related to climate predictability (Griffies and Bryan, 1997) and an accurate projection of anthropogenic climate changes. Roemmich and Wunsch (1984) reported variability in the North Atlantic Deep Water formation rate; Kushnir (1994) found multidecadal variability of the sea surface temperature (SST) and the sea level pressure (SLP) in the CODAS dataset. A similar variability can be found in atmosphere-ocean coupled climate models. Delworth *et al.* (1993) observed interdecadal variation in the North Atlantic thermohaline circulation, which is supposed to be an atmosphere-ocean coupled process caused by stochastic noise from the atmosphere and thermal inertia of the ocean (Hasselmann, 1976; Delworth and Greatbatch, 2000; Delworth and Mann, 2000).

To isolate the main processes governing such variability many numerical studies have been conducted under simplified conditions. From idealized modeling studies in which the ocean circulation is driven by a steady heat flux, Greatbatch and Zhang (1995), Cai *et al.* (1995), Cai and Chu (1996), Winton (1996) and Greatbatch and Peterson (1996) have shown that interdecadal variability similar to that from the coupled climate model by Delworth *et al.* (1993) can be generated spontaneously in an ocean-only model. Such oscillations are robust so they are found in a model coupled to thermodynamic ice models (Kravtsov and Ghil, 2004). The process that is mostly commonly related to the variability is a relationship between the meridional overturning and meridional temperature or density gradient.

Greatbatch and Zhang (1995) suggested that when the overturning is stronger than average, the heat transport to high latitude increases. The meridional temperature gradient subsequently weakens to reduce meridional heat transport to high latitudes. The meridional temperature gradient becomes greater again to enhance the overturning and starts the cycle again. This explanation is consistent with the model results, but it does not guarantee variability. For example, if the THC anomaly and the temperature anomaly are in phase, the anomalies interfere destructively and the variability cannot be sustained. Huck *et al.* (1999; HCW hereafter), who extensively investigated the effects of various parameters on variability, suggested that a phase difference between meridional temperature gradient and the strength of the meridional overturning is crucial to the variability. Colin de Verdière

and Huck (1999) and Arzel *et al.* (2006) suggested that under a flux boundary condition the propagation of temperature anomalies and the subsequent response of the flow are crucial in establishing the phase relation, but no clear explanation of the physics underlying such a phase relation has been given.

Te Raa and Dijkstra (2002; TD hereafter) and Dijkstra (2006) also argued that the crucial elements in the variability are: 1) the phase difference between the zonal and meridional surface flow perturbations; and 2) the westward propagation of the temperature anomalies as in the aforementioned studies. A warm anomaly in the north-central part of the basin weakens the meridional temperature gradient which in turn induces a negative zonal surface flow anomaly. In addition, the anomalous anticyclonic circulation around the warm anomaly causes southward (northward) advection of cold (warm) water to the east (west) of the anomaly, resulting in westward propagation of the warm anomaly. As a result of this westward propagation, the zonal perturbation temperature gradient becomes negative, inducing a negative surface meridional flow. The resulting upwelling and downwelling anomalies along the northern and southern boundaries, respectively, enhance the meridional temperature gradient, inducing a positive zonal surface flow, and the second half of the oscillation starts. In Te Raa *et al.* (2004) and Dijkstra *et al.* (2006) the westward propagation of temperature anomalies and the phase difference between the anomalous zonal and meridional overturning are considered to be a fingerprint of interdecadal internal variability.

There is no doubt that the propagation of temperature anomalies and the subsequent response of flow fields are crucial. However, a few concerns require further clarification. First, the anomalous anticyclonic circulation around the warm anomaly mainly follows the isotherms and cannot transport any heat. In other words, a flow simply circumscribes the anomaly would be developed, and the anomaly cannot propagate to the west.

Secondly, TD relies on globally averaged properties such as overall zonal and meridional overturning circulations to explain the behavior of anomalies with strong zonal and meridional variations. (See Fig. 4 of this paper or figure 9 of HCW, which show the evolution of temperature and velocity anomalies at the surface during an oscillation cycle.) For example, a negative zonal overturning, which pushes warm anomalies to the west along the northern wall according to TD, does not necessarily mean that such a circulation pattern is found near the northern boundary. Furthermore, how does the global negative zonal overturning that is obtained from meridional average become active only along the northern wall?

Thirdly, anomalies do not form near the eastern boundary but they do form near the western boundary,

and expand to the east while intensifying, as shown by HCW or Colin de Verdière and Huck (1999). Anomalies start to propagate to the west only after they encounter the northern wall, as shown later in this paper or in HCW. The mechanism provided by TD is incomplete because the eastward propagation is not considered, even though we accept their explanation.

In this paper, using idealized numerical experiments that are similarly configured to earlier studies, such as Winton (1996), we investigate the structure of thermal variability. We do not intend to report a new type of variability, but to propose a self-sufficient mechanism that does not rely on *a priori* assumption or a relation between zonally or meridionally averaged diagnostic quantities. Our newly proposed mechanism relies on the local interaction among temperature anomalies, horizontal velocity anomalies induced by the temperature anomalies, and the continent blocking the velocity anomalies (Winton, 1996; Park, 2006) to explain the westward propagation of the anomalies. Anomalous flows developed by a temperature anomaly induce another temperature anomaly of the opposite sign, propagating cyclonically over the northern part of the basin by enhancing or reducing temperature advection. By relating changes in the meridional temperature gradient, which is due to the westward propagation of anomalies as in TD, not to those of overall zonal overturning but to those of local zonal flows, we explain the eastward propagation of anomalies.

Our mechanism is based on the localized interaction of anomalies, and we do not need to invoke the phase relation between the meridional overturning and temperature gradient. Such a relationship, however, can be used as a fingerprint of interdecadal internal variability (Te Raa *et al.*, 2004; Dijkstra *et al.*, 2006), and we explain how such a relation is established as a “*consequence*” of the variability using our mechanism of the variability.

To sustain the variability, energy must be supplied externally. Since buoyancy is the only forcing, the available potential energy, of course, should be released through buoyancy work and converted into kinetic energy, as stated by TD. However, energy flows are different depending on the processes controlling the variability. For example, if baroclinic instability is mainly responsible for the variability, as suggested by Colin de Verdière and Huck (1999) and Arzel *et al.* (2006), the energy stored in the mean stratification should be converted. To illustrate the energy flow, we conducted an energy analysis similar to that described in TD following the method by Haidvogel and Beckmann (1999), and found that the variability is maintained by the release of the available potential energy stored in the anomalous density field through the anomalous buoyancy work, mainly over the northeastern corner of the basin. Thus, neither baroclinic nor barotropic instability is responsi-

ble for the variability. In addition, we describe the temporal behavior of the buoyancy work in conjunction with the interaction between anomalies and the wall.

The vertical velocity anomaly that mainly governs the buoyancy work is strongest along the northern wall and the northern part of the eastern wall where the water is well mixed due to convection (Park and Bryan, 2001). Thus, if our energy analysis is correct, the variability could be weakened by reducing vertical velocities over those areas.

We then utilize our energy analysis to explain the weakening effect of bottom topography on variability, as reported in earlier studies (Winton, 1997; Huck *et al.*, 2001; Te Raa *et al.*, 2004). Winton (1997) argued that with the presence of a bowl shaped geometry, the bottom pressure torque would modify the strength of the meridional overturning circulation and thereby suppress variability. According to Park and Bryan (2000), however, if the zonal mean is taken along an isopycnal surface instead of level surfaces, the overall shape of the overturning circulation in a flat bottom case is not significantly different from that of a bowl-shaped bottom case. Therefore, meridional overturning may not properly reveal the effects of bottom topography on thermohaline variability. The bottom topography, however, modifies the high latitude circulation quite drastically by prohibiting vertical motion along boundaries in high latitude, as discussed by Park and Bryan (2001). The vertical velocity anomaly mainly governs the buoyancy work, and if our energy analysis is correct, one could weaken the variability by reducing vertical velocities over those areas. To this end, we consider cases with a continental shelf along individual boundaries, and a case with the continental shelf along all the boundaries except the southern one. We show that a continental shelf along the eastern or northern boundary significantly weakens the variability by reducing the buoyancy work, while one along the western boundary cannot exert much influence on the buoyancy work and the variability. Previous studies have not considered the effects of the individual boundary.

The outline of this paper is as follows: Section 2 describes the design and procedure of idealized numerical experiments. Model results are discussed in Section 3 along with the mechanism that drives the variability and the energetics of the variability. The effects of the bottom topography and the surface heat flux pattern on the variability are also described. Section 4 gives a brief summary and conclusions.

2. Design

The NOAA/GFDL Modular Ocean Model V.3 has been used in this study. The model domain is a spherical sector bounded by meridional planes 60° apart and zonal planes at the equator and 60°N . The horizontal resolution

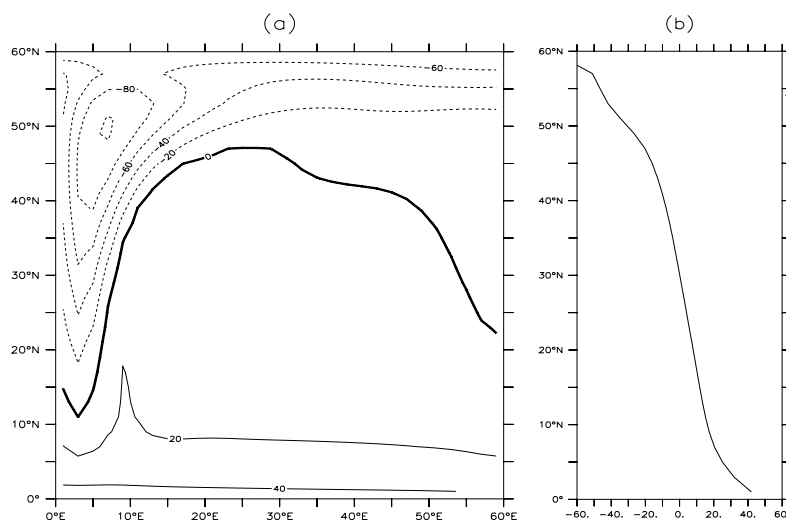


Fig. 1. (a) Surface heat flux pattern diagnosed from a run with a restoring boundary condition, and (b) its zonal average. Units are Wm^{-2} in both cases. The pattern shown in (a) is used in FLUX as the surface boundary condition and that in (b) in all other cases.

Table 1. Summary of the experiment. Here 2D stands for the two dimensional heat flux pattern shown in Fig. 1(a), and 1D the zonal mean of 2D shown in Fig. 1(b).

CASE	Forcing	Location of a shelf
FLAT	1D	no
BOWL	1D	E, N, W
EAST	1D	E
NORTH	1D	N
WEST	1D	W
FLUX	2D	no

is 2° in both zonal and meridional directions. To investigate the role of bottom geometry, five types of bottom geometry are considered: FLAT, EAST, NORTH, WEST and BOWL as listed in Table 1. FLAT uses a flat bottom geometry of 4 km depth. In EAST, NORTH and WEST, a sloping bottom that deepens gradually from 200 m at the side wall to 4000 m at the 13th grid point (i.e., 26°) from the wall is considered along the eastern, northern and western boundaries, respectively. In BOWL, the sloping shelf exists along the boundaries except the southern, i.e., the equatorial boundary. There are 20 vertical levels and the thickness of the levels is 25 m for the upper 200 m, increasing up to 608 m thereafter. The quicker advection scheme is used. A linear equation of state is used and temperature and density are equivalent. The vertical diffusivity $\kappa_v = 1 \times 10^{-4} \text{ m}^2\text{s}^{-1}$ throughout the domain. Variabilities occur when the horizontal diffusivity κ_H is lower than a certain value (HCW), and $\kappa_H = 1 \times 10^3$

m^2s^{-1} , which is comparable to what HCW used.

It is easier to obtain variability with a flux boundary condition (Colin de Verdière and Huck, 1999), and the motions are driven by steady heat fluxes applied at the surface in the absence of surface wind stresses. To obtain surface heat fluxes that are compatible with the model configuration, the model with FLAT configuration was first integrated for 3000 years under a restoring boundary condition with a 30 day restoring scale, after which the surface mean heat flux is diagnosed (Fig. 1(a)). In this run, no meaningful variability was observed. To keep the forcing as simple as possible, the zonal mean of the diagnosed heat flux (Fig. 1(b)) is used as the surface boundary condition in all cases except in FLUX, in which the heat flux shown in Fig. 1(a) is used to investigate the sensitivity of variability to heat flux pattern proposed by Cai *et al.* (1995). With the surface heat fluxes, the model was integrated for 3200 years to exclude any transient phenomena in each case. Results from the last 200 years are used in the analysis.

3. Results

3.1 Variability mechanism

Figure 2 shows a time series of the basin volume mean kinetic energy

$$KE = \rho_0 \langle u^2 + v^2 \rangle / 2,$$

where u is the zonal and v the meridional velocities, ρ_0 is the mean density, and a bracket, $\langle \rangle$, represents a basin

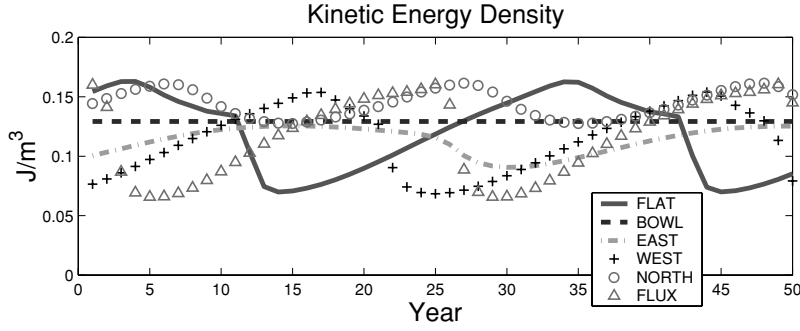


Fig. 2. Temporal variation of total kinetic energy density obtained through averaging over the entire basin for each case.

Table 2. Energetics from each case. See the text for the definition of the quantities. The unit for energy (*APE* and *KE*) is kg/ms^2 and that for the conversion rate (T_1 through T_4) is kg/ms^3 .

	FLAT	BOWL	EAST	NORTH	WEST	FLUX
<i>MAPE</i>	106	62	108	115	97	123
<i>EAPE</i>	20	0	5.4	1.4	21	15
<i>EAPE/MAPE (%)</i>	19	0	5	1.2	22	12
<i>MKE</i>	0.12	0.14	0.12	0.15	0.11	0.11
<i>EKE</i>	0.013	0	0.0034	0.0014	0.011	0.0098
<i>EKE/MKE (%)</i>	11	0	2.8	0.9	9.7	8.7
<i>MAPE</i> \rightarrow <i>MKE</i> : T_1	1.6×10^{-7}	4.1×10^{-7}	2.2×10^{-7}	3.1×10^{-7}	1.9×10^{-7}	1.8×10^{-7}
<i>MAPE</i> \rightarrow <i>EAPE</i> : T_2	-0.35×10^{-7}	0	-0.89×10^{-7}	-0.03×10^{-7}	-0.32×10^{-7}	-0.41×10^{-7}
<i>EAPE</i> \rightarrow <i>EKE</i> : T_3	0.24×10^{-7}	0	0.07×10^{-7}	0.005×10^{-7}	0.22×10^{-7}	0.16×10^{-7}
<i>MKE</i> \rightarrow <i>EKE</i> : T_4	0	0	0	0	0	0

volume mean. There are, of course, other ways of defining the characteristics of variability (HCW, for example), but the *KE* shows the characteristics very well (Winton, 1997). To quantify the strength of the variability, the *KE* is divided into time-mean component,

$$MKE = \rho_0 \langle \bar{u}^2 + \bar{v}^2 \rangle / 2,$$

where a bar, $\bar{}$, represents a mean over the period of the variability, and a temporally fluctuating component, the eddy kinetic energy

$$EKE = \rho_0 \langle u'^2 + v'^2 \rangle / 2,$$

where a prime ' means deviation from the time mean. (The fluctuating components are not eddies, but they are deviations from the time mean and are conceptually similar to eddies.) The results are listed in Table 2 along with other properties explained later. Figure 2 and the *EKE* level in the table clearly indicate that FLAT shows the

strongest variability, with a period about 32 years long, and BOWL shows no variability at all, as in Winton (1997). The *EKE* level or its ratio to the *MKE* from EAST or NORTH is significantly weaker than that from FLAT, but the one from WEST is comparable to that from FLAT. We explain later why the topography along the western boundary does not suppress the variability notably while ones along other boundaries do. Since FLAT shows strongest variability, the results from this case have been investigated.

The mean circulation pattern and SST at the surface from FLAT are shown in Fig. 3, and SST and velocity anomalies during an oscillation cycle over the northern half of the basin, where the variability is more prominent, are shown in Fig. 4. The evolution of the anomalies is similar to those in earlier studies, especially figure 9 of HCW or figure 2 of Colin de Verdière and Huck (1999). Detailed analysis of model results can be found in those earlier studies, so a similar analysis will not be repeated here. Instead, we focus on explaining the mechanism of the variability.

To understand the structure of the variability, we need

to know the mean surface circulation pattern. As shown by Park and Bryan (2001), there is a northward western boundary current that carries warm water from the south to the north so that the western boundary layer is warmer than the interior. At the same time, the meridional temperature gradient at the surface drives an eastward zonal flow. Of course, the above description is a rough, general trend. When the zonal flow meets the eastern wall, most of the water sinks to the subsurface level and returns to the west. The remaining small part turns to the north. Since the zonal flow transports warm water from the western boundary to the eastern boundary, a positive (negative) zonal flow anomaly induces a warm (cold) temperature anomaly along the path of the mean zonal flow, and a downwelling (upwelling) anomaly over the northeastern corner.

A diagram of the structure of variability is presented in Fig. 5. Assume that a cold anomaly is formed along the northern boundary (cold phase, Year 30 in Figs. 4 and 5). This cold anomaly strengthens the meridional temperature gradient (T_y in Fig. 5 where y increases to the north) over the high-latitude ocean, and subsequently the eastward zonal flow, which transports warm water from the west to the east, becomes stronger. Therefore a warm anomaly is formed to the south of the cold anomaly (Year 32 in Fig. 4). The meridional temperature gradient anomaly is intensified further, so does the positive zonal flow anomaly and the warm anomaly propagates to the east along the path of the zonal flow. The eastward propagation of the warm anomaly can be seen more clearly by tracing the boundary between the warm anomaly and the cold anomaly, the zero degree isotherm. Comparing the zero degree isotherms from Year 30 and Year 32, one can see that the head of the warm anomaly moves to the east with an average speed of about 3 cm/sec, which is comparable to the magnitude of the mean zonal flow shown in Fig. 3. The importance of horizontal heat advection from the tropical area to the subpolar area in thermohaline variability has been noticed already (Yin and Sarachik, 1995; Colin de Verdière and Huck, 1999), but the fact that the advection could modify the temperature gradient that drives the advection has not attracted much attention. The zonal flow is from the western boundary current, and the western boundary current anomaly is linked to the zonal flow anomaly. As the zonal flow anomaly becomes stronger (or weaker), so does the western boundary current anomaly, as can be seen in Fig. 4 (Years 2 and 6, for example).

When the zonal flow encounters the eastern wall (Year 2 in Fig. 4), the water sinks to subsurface level in the horizontal Ekman layer (Winton, 1996) of thickness $(2A/f)^{1/2} \approx 40$ km when the lateral viscosity $A = 2 \times 10^5$ m²s⁻¹, and the Coriolis parameter $f = 10^{-4}$ s⁻¹. The layer is thinner than the horizontal resolution, which is 2°, and

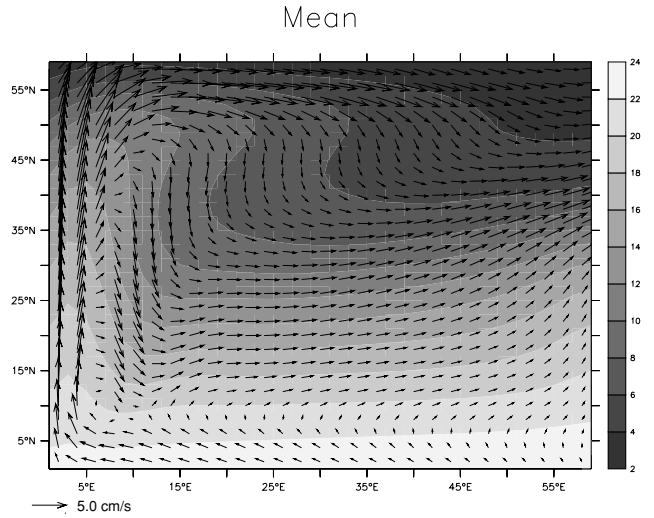


Fig. 3. Mean surface circulation and SST distribution patterns from FLAT.

the downwelling occurs along the easternmost grid points. Figure 6(a) shows a time series of vertical temperature gradient profile in the easternmost grid point at 50°N. From the surface to about 1000 m deep, the water is very well mixed due to convection. The thickness of the mixed layer does not change much over time so it can be simplified as a homogeneous layer of fixed thickness h . In a steady state, the dominant terms near the eastern boundary are the Coriolis term, the pressure gradient term, and the viscosity (Sumata and Kubokawa, 2001). If a temporal term due to the variability is added,

$$\frac{\partial \mathbf{u}}{\partial t} + f \mathbf{k} \times \mathbf{u}_H = -\nabla p + A \nabla^2 \mathbf{u}. \quad (1)$$

Here, horizontal velocity $\mathbf{u}_H = (u\mathbf{i} + v\mathbf{j})$, \mathbf{i} , \mathbf{j} , \mathbf{k} are the unit vectors in the zonal, meridional, and vertical directions, respectively, and p is pressure normalized to a reference density. If we take the curl of the above equation, we get a vorticity equation

$$\frac{\partial \zeta}{\partial t} + \beta v - f \frac{\partial w}{\partial z} - A \nabla^2 \zeta = 0, \quad (2)$$

where relative vorticity $\zeta = \mathbf{k} \cdot \nabla \times \mathbf{u}_H$, w is vertical velocity, and β is the planetary vorticity gradient. If we decompose the variables into the time means and the perturbations, we get a vorticity equation for the variability as follows:

$$\frac{\partial \zeta'}{\partial t} + \beta v' - A \nabla^2 \zeta' = f \frac{\partial w'}{\partial z}. \quad (3)$$

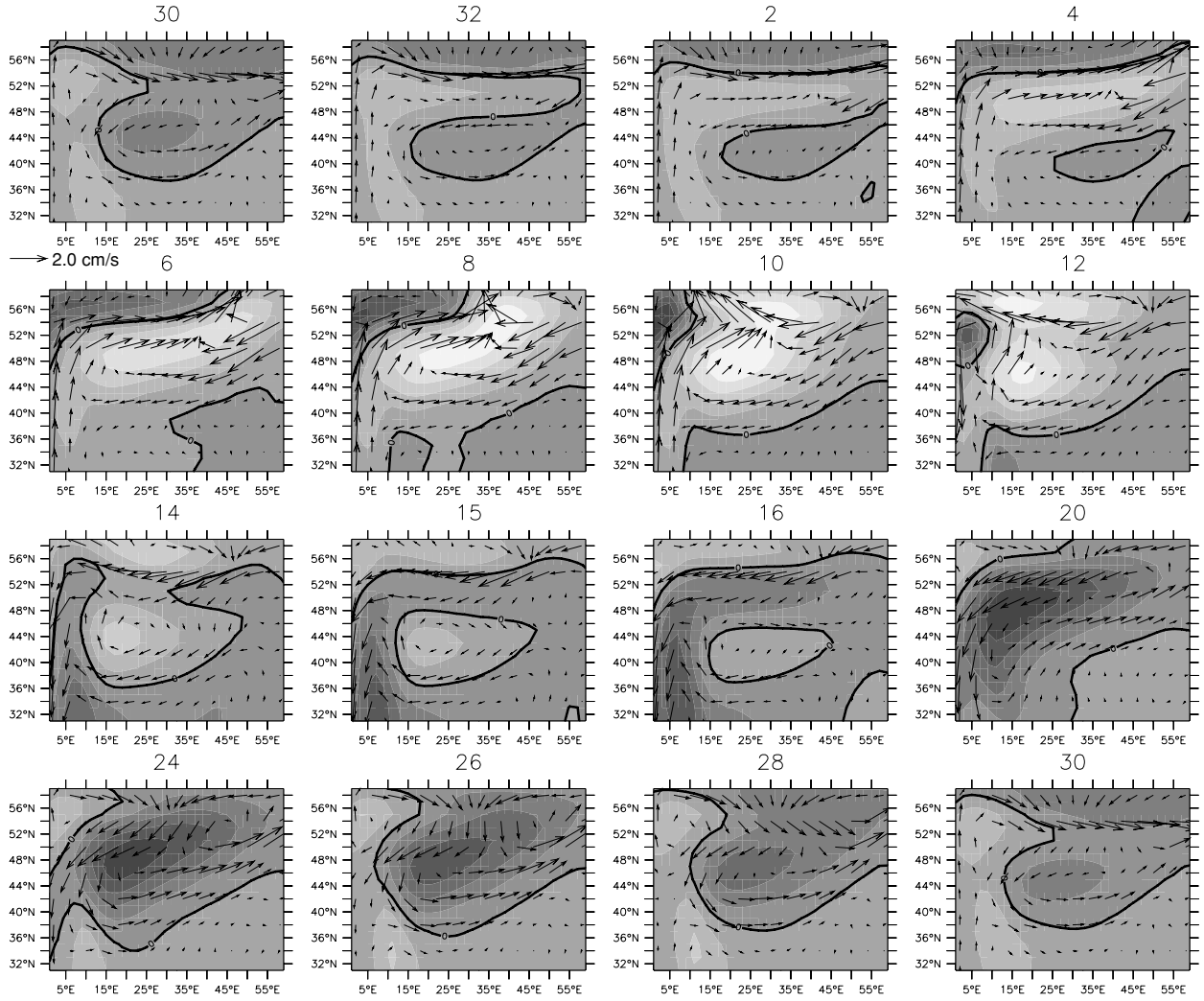


Fig. 4. Evolution of surface temperature (grey scale shading in 0.4°C interval) and velocity anomalies (arrows) from FLAT over the northern half of the basin. Darker shading means cooler water. Numbers represent years during a variability cycle.

Here, primed variables represent perturbation quantities. The above relation is similar to that of Winton (1996) except here the β term and the temporal derivative are added.

Within the mixed layer near the eastern wall, when $u' > 0$, the downwelling strengthens with depth, and $\partial w' / \partial z > 0$ (Fig. 6(c)). The vortex column stretching (*r.h.s* in Eq. (3)) should be balanced by the sum of the production of positive relative vorticity, an increase in the planetary vorticity ($\beta v'$), and the frictional dissipation. Because the downwelling occurs over the easternmost grid point, the zonal length scale Δx is the zonal resolution, which is $2^\circ \sim O(10^5 \text{ m})$, and is much smaller than the meridional scale. This means that the magnitude of the frictional term is

$$\frac{A \partial^2 \zeta'}{\partial x^2} \approx \frac{A V'}{\Delta x^3} \approx O(10^{-10} \text{ s}^{-1} \text{ m}^{-1}) V',$$

where V' is a scale for the meridional velocity induced by the downwelling. The magnitude of $\beta v'$ is comparable to that of the frictional term since the lateral eddy viscosity A is set to satisfy the Munk boundary layer thickness $\delta_M = (A/\beta)^{1/3} \approx \Delta x$. However, the magnitude of the time derivative, $\partial \zeta' / \partial t \approx V' / \Delta x T \approx O(10^{-14} \text{ s}^{-1}) V'$, where T , the period of variability, is $O(30 \text{ years})$, is much smaller than the frictional term. Therefore, the vortex column stretching should be balanced by northward movement and friction at the eastern wall. Since the downwelling at the eastern wall is caused by the zonal flow anomaly, from the continuity equation we estimate that $W'/H \approx U'/\Delta x$, where U' is a scale for the zonal flow anomaly. Then,

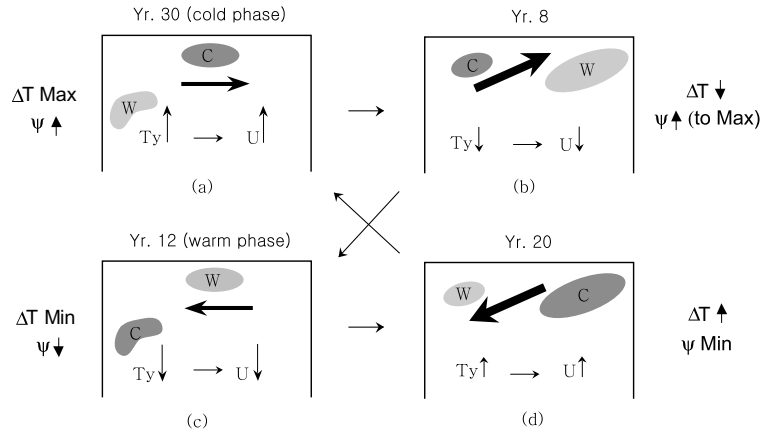


Fig. 5. Diagrams of the dynamics of the variability. “W” is for a warm anomaly, and “C” for a cold one. Arrows indicates velocity anomalies due to temperature anomalies. Here, T_y is the mean meridional temperature gradient over the northern part of the basin, while y increases to the north, “U” is the magnitude of the zonal flow at the surface induced by T_y , ΔT means the overall (equator to pole) meridional temperature difference, Ψ the strength of the overturning. Numbers represent corresponding years in Fig. 4.

$$\beta V' \approx A \frac{V'}{\Delta x^3} \approx f_0 \frac{W'}{H} \approx f_0 \frac{U'}{\Delta x},$$

so

$$V' \approx \frac{f_0}{\beta \Delta x} U' \approx \frac{f_0 \Delta x^2}{A} U' \approx O(U'). \quad (4)$$

A northward flow with amplitude comparable to that of the zonal flow anomaly is produced when the zonal flow encounters the eastern wall, as can be seen in Fig. 6(d). To balance the positive tendency, the β term induces a northward flow at the eastern wall. In addition, the frictional term, the magnitude of which is set to be comparable to that of $\beta v'$, requires a production of negative relative vorticity. It then produces a northward flow to satisfy the no-slip boundary condition at the eastern wall (Park, 2006).

As can be seen from Fig. 6, the stronger the zonal flow anomaly, the greater is the downwelling, and consequently the meridional flow anomaly becomes that described by Eq. (4). The northward flow anomaly and the zonal flow anomaly are concurrent, and the former transports the latter northward along the eastern wall. An accompanying downwelling anomaly is induced at higher latitude, and so is a northward flow anomaly according to Eq. (4). Therefore, the positive zonal flow anomaly continues to move northward along the boundary. If the zonal flow anomaly is negative, the vortex column shrinks and a southward movement along the boundary would be induced, as shown in Fig. 6(d). Further explanation of this northward flow along the eastern boundary in re-

sponse to the downwelling is given in Park (2006).

Instead of investigating the vorticity balance, Winton (1996) assumed *a priori* that a Kelvin wave-type process would govern the adjustment near the wall, and utilized a linearized frictional geostrophic shallow water system. By observing the propagation of temperature anomalies away from boundary, HCW argued that the viscous “Kelvin” waves are not important. Since the Kelvin wave-type interaction is not used to explain interior propagation but rather the interaction of an anomaly with a boundary, Winton’s (1996) argument may be applicable, if it is confined to the area near boundaries.

Excluding the β term, which is not crucial to the variability according to HCW, and the temporal term, which is smaller than the other terms, Eq. (3) takes the same form as that of Winton (1996). Thus, in both the current analysis and that of Winton (1996), lateral friction is found to be the main dissipation process. Our approach, however, is more straightforward since we utilized the vorticity equation directly. In addition, we propose a mechanism that can explain the propagation of an anomaly away from boundaries.

The northward flow formed at the eastern boundary due to the vortex column stretching continues cyclonically along the boundaries and supplies warm water to the northern area while pushing the cold anomaly to the west, as sketched in Fig. 5(b) or as seen in the model results (Years 4 and 6 in Fig. 4). Note that when the anomaly reaches the northern wall the β term no longer exists, and a viscous boundary forms along the northern wall. Therefore, if we replace variables related to the zonal coordinate by those related to the meridional coordinate in Eq. (4), and vice versa, we get a zonal velocity scale of

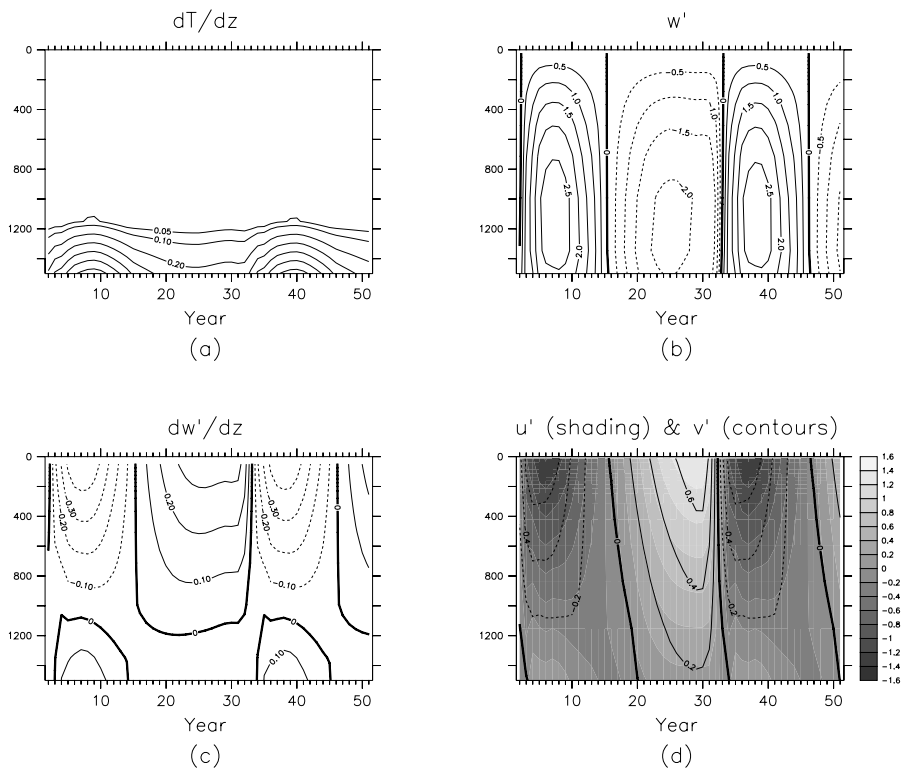


Fig. 6. Time series of the vertical distribution of (a) vertical temperature gradient ($\partial T/\partial z$) in $^{\circ}\text{Cm}^{-1}$, (b) the vertical velocity anomaly (w') in 10^{-5}ms^{-1} , (c) the vertical shear of the velocity anomaly ($\partial w'/\partial z$) in 10^{-7}s^{-1} , and (d) the zonal (u' , shadings) and meridional (v' , contours) velocity anomalies in 10^{-2}ms^{-1} in the easternmost grid points at 50°N .

an anomaly along the northern wall $U' \approx (f_0 \Delta y^2 / A) V' \approx O(V')$. Here V' is the speed of the meridional flow anomaly that downwells within the viscous boundary layer. The downwelling anomaly (Fig. 6(b)) accompanies the positive zonal flow anomaly (Fig. 6(d)), which transports the downwelling anomaly to the west, and the cyclonic propagation of the anomaly continues (Fig. 7). Note that the northward flow is weaker than the zonal flow since only a part of the zonal flow would turn northward (Fig. 6(d)), and it would take longer for an anomaly to move to the west along the northern boundary than to move to the east cross the basin by the mean zonal flow. It takes about two years for the warm anomaly to move about 30° along the 52°N latitude line (between Years 30 and 32), while it takes about four years for the head of the warm anomaly to move about 30° along the northern boundary (between Years 4 and 6).

TD and Dijkstra (2006) argued that the anomalous anticyclonic circulation around a warm anomaly causes southward (northward) advection of cold (warm) water to the east (west) of the anomaly, resulting in westward propagation of the warm anomaly. As mentioned earlier, the anomalous flow due to the thermal wind relation follows the isotherms, and the flow cannot transport any heat

nor make the anomaly propagate. In other words, the flow simply circumscribes the anomaly would be developed if the aforementioned interaction of the flow with the boundary is not considered. In addition, the mechanism proposed by TD fails to provide any explanation of the eastward propagation of the anomalies across the basin.

While the tip of the warm anomaly moves cyclonically along the boundary, its tail does not interact with the boundary and does not propagate significantly. The anomaly pivots with the center at the tail so that the zonally aligned anomaly at Year 2 becomes a meridionally aligned one at around Year 10. The anomalous flow is mainly in the meridional direction and perpendicular to the mean temperature gradient. The flow becomes more effective in creating a temperature anomaly, and the anomaly strengthens.

Warm water eventually fills the high latitudes (warm phase, Year 12 in Fig. 4 for example) and the meridional temperature gradient weakens, producing a negative zonal flow anomaly, as sketched in Fig. 5(d). A negative zonal flow anomaly means that the warm advection is reduced so that a cold anomaly is produced along the path of the anomalous zonal flow to the south of the warm anomaly. Near the eastern wall, the temperature anomalies are ori-

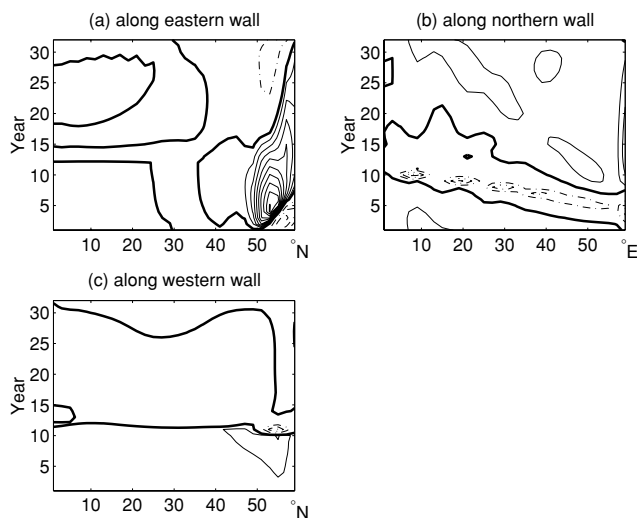


Fig. 7. Hovmuller map of vertical velocity anomaly (w') in 10^{-5} ms^{-1} along the eastern, northern and western walls at 100 m deep along the (a) the eastern, (b) the northern, and (c) the northern walls. The same pattern is observed at other depths. For negative values (dashed dotted lines) the contour interval is 1, and for positive values (thin solid lines) 0.2. Thick solid lines represent 0.

ented meridionally (see 0.4 degree isotherm in Year 10 or 12 in Fig. 4), and subsequent southeastward flow anomalies are very effective in reducing the advection of warm water or, equivalently, generating cold anomalies. Therefore cold anomalies start to form both from the western and eastern walls. The anomalies expand into the interior along the 50°N line (Year 14 of Fig. 4), and merge in between to form a zonally aligned cold anomaly across the basin (Year 15 of Fig. 4). Since the cold anomaly starts from both ends of the basin, it takes less time to form a cold anomaly across the basin. As shown by the -0.4°C isotherm in Year 16, the main part of the cold anomaly is from the west. If no cold anomaly were arriving from the east, it would take longer for the cold anomaly to cross the basin. This cold anomaly strengthens the negative meridional temperature gradient anomaly, and subsequently the negative zonal flow anomaly. The warm advection is reduced even further and the cold anomaly strengthens. The western boundary anomaly is linked to the zonal flow anomaly and the western boundary current is also weakened.

On encountering the eastern wall, the negative zonal flow anomaly weakens downwelling and induces an upwelling anomaly near the eastern wall (Fig. 6). Vortex column shrinking occurs to induce a southward flow anomaly (Eq. (4)). The southward flow then supplies water to the area of the negative zonal flow anomaly to reduce the upwelling anomaly, and weakens the north-

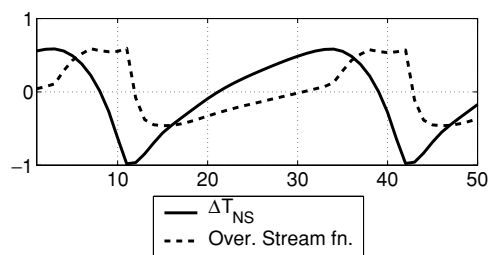


Fig. 8. Phase relation between the maximum of the meridional overturning circulation anomaly (dashed line) and the mean north-south temperature difference anomaly (solid line) from FLAT in arbitrary scales.

ward transport of warm water along the eastern wall. A cold anomaly would be produced to the north of the upwelling anomaly. Downwelling would be reduced over the newly formed cold anomaly because the water used to downwell is transported southward, and an upwelling anomaly would be produced, which in turn induces southward flows. Thus, a cold anomaly and accompanying upwelling and negative flow anomalies (Fig. 7) propagating cyclonically along the perimeter of the basin along while pushing the warm anomaly would be formed (Year 20). Note that upon reaching the northern wall, the negative zonal flow anomaly becomes a negative meridional flow anomaly, and an eastward flow anomaly would be induced instead of a southward flow anomaly. The speed of propagation of the upwelling anomaly is $1/3$ to $2/3$ that of the downwelling anomaly. The cold anomaly eventually fills the northern boundary (Year 26), and produces a positive meridional temperature gradient anomaly (Year 30) and a cycle is completed. Thus, the cycle of the variability is determined by multiple advection time scales. While crossing the basin to the east the anomaly is mainly transported by the mean flow. Upon reaching the eastern wall, the anomaly is transported by the anomalous flows induced by the interaction between the temperature anomaly and the walls.

3.2 Phase relation

Figure 8 shows a comparison between the meridional overturning circulation anomaly and the mean north-south temperature difference anomaly during an oscillation cycle. Here the meridional overturning is defined along depth level surfaces. The evolution of the overturning streamfunction Ψ during an oscillation cycle is shown in Fig. 9. As in previous studies (Delworth *et al.*, 1993; Kravtsov and Ghil, 2004; Te Raa *et al.*, 2004, for example), the meridional temperature gradient anomaly leads the meridional overturning circulation anomaly. Although we do not need such a relationship to explain the variability, it can be used as a fingerprint of interdecadal in-

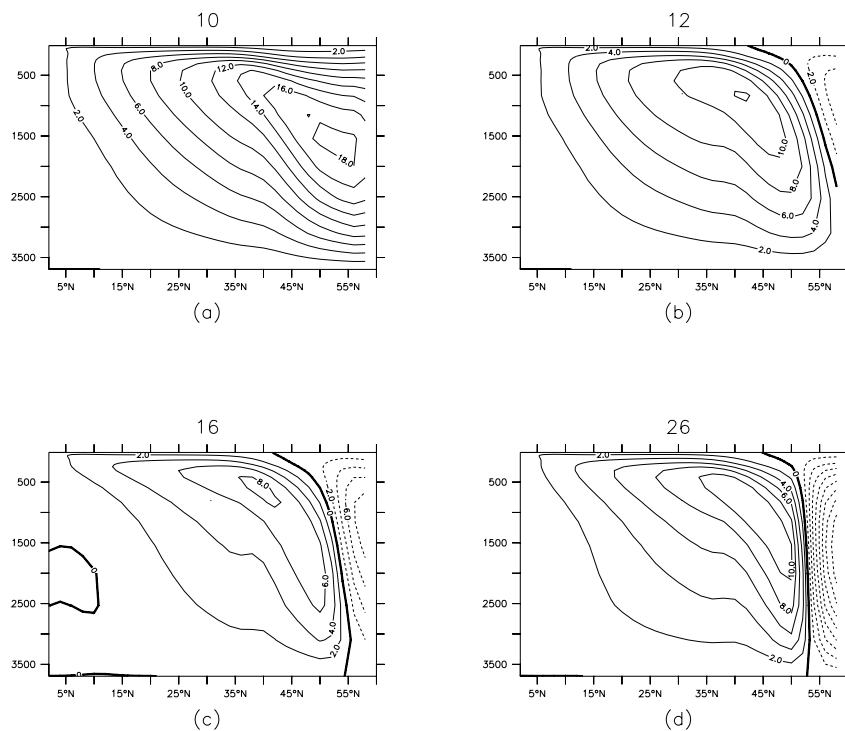


Fig. 9. Evolution of the meridional overturning streamfunction during an oscillation cycle from FLAT.

ternal variability (Te Raa *et al.*, 2004; Dijkstra *et al.*, 2006). Therefore, we explain how the phase relation is established through local interplay between the positioning of anomalies and accompanying horizontal flow anomalies.

Our explanation is similar to that of TD, because the meridional temperature gradient changes as a consequence of the propagation of temperature anomalies. In TD, the meridional temperature gradient is then related to meridional overturning through zonal overturning and zonal temperature gradient. It is certain that zonal (meridional) overturning would become stronger if meridional (zonal) temperature gradient intensifies. According to Cai *et al.* (1995), however, the variability has a three-dimensional character, and even under the same zonally averaged forcing the mean meridional overturning can differ depending on the zonal structure of the forcing. In addition, it is not clear if the response of the zonal (meridional) overturning to changes in meridional (zonal) temperature gradient is immediate or delayed. If it is delayed, we need other relationships to explain it. Thus, TD's argument relating meridional temperature to meridional overturning may not be straightforward. We, however, obtain meridional overturning from horizontal velocities induced by temperature anomalies directly, independent of the temperature gradient.

At Year 2 in Fig. 4, since we have a cold anomaly at

the north, the overall meridional temperature gradient or difference, ΔT in Fig. 5(a), is at or near its maximum. The flow anomaly, which is mostly zonal due to zonally aligned temperature anomalies, is principally found in changes in the speed of the western boundary and induces a positive western boundary current anomaly. This produces a weak positive meridional overturning anomaly, as in Fig. 8. As the warm anomaly pivots cyclonically (Year 6 in Fig. 4 or Fig. 5(b)), the meridional velocity component and subsequently the meridional overturning circulation becomes stronger while the meridional temperature gradient weakens since more warm water is supplied to the northern area. At Year 10 in Fig. 4, the temperature anomalies are aligned more or less meridionally, and the velocity anomalies are mainly in the meridional direction. Therefore, the maximum of the meridional overturning is achieved (Fig. 9(a)) a few years after the maximum of the meridional temperature gradient is reached (Fig. 8). Note that there is a southward flow along the eastern side of the warm anomaly in addition to the northward flow along the western side. Since the temperature gradient is larger on the side neighboring the cold anomaly, the northward flow to the west of the warm anomaly is greater than the southward flow to the east.

At Year 12 in Fig. 4, the northern area is more or less filled with warm water and the meridional temperature gradient, or equivalently ΔT , is at its minimum. Due

to the weakening of the cold anomaly over the northwestern corner, the northward flow on the western side of the warm anomaly, and subsequently the western boundary current anomaly are reduced. Therefore the meridional overturning weakens toward the minimum. The weakening of the cold anomaly makes the southward flow to the east of the warm anomaly stronger than the northward one to the west, and if we take a zonal mean along level surfaces a reverse overturning circulation cell is obtained near the northern wall (Fig. 9(b)). At Year 16 in Fig. 4, the warm anomaly has almost disappeared and the meridional temperature gradient starts to strengthen toward the maximum. Meanwhile, the zonally aligned warm and cold anomalies produce a negative zonal flow anomaly. The zonal flow is from the western boundary current so that the negative zonal flow anomaly induces a negative western boundary current anomaly, resulting in the minimum of the overturning (Fig. 9(c)).

As time progress, the cold anomaly becomes stronger while propagating to the east. Once the center of the anomaly detaches from the western boundary, the anomalous flow is mostly around the temperature anomaly (Year 26 in Fig. 4, for example). The negative western boundary current anomaly is reduced and the meridional overturning starts to intensify. Similar to the case of the developed warm anomaly (Year 10), the temperature gradient is larger on the western side of the cold anomaly due to the warm anomaly located over the northwestern corner. The southward component to the west of the anomaly is stronger than the northward one to the east, and the net is southward. As the cold anomaly becomes stronger while pivoting cyclonically (from Year 16 to Year 26 in Fig. 4), the mean zonal temperature gradient to the north of 50°N or so attains a greater negative value, and the southward velocity component strengthens, producing an intensified negative overturning cell. The negative cell weakens later, when the temperature anomalies align zonally.

3.3 Energetics

Since friction dissipates energy, the energy maintaining the variability must be supplied externally. The heat flux at the surface is the only forcing, and the available potential energy stored in the stratification should be converted into kinetic energy, as stated by TD, by buoyancy work. The energy supplied by the forcing, however, can take different paths before being dissipated by the friction, depending on the processes controlling the variability. As suggested by Colin de Verdière and Huck (1999), TD, and Arzel *et al.* (2006), if baroclinic instability is mainly responsible for the variability, the energy stored in the mean stratification should be converted. One of the important processes in the mechanism we proposed for the variability is anomalous vertical motion near the walls at high latitude. Since this anomalous vertical mo-

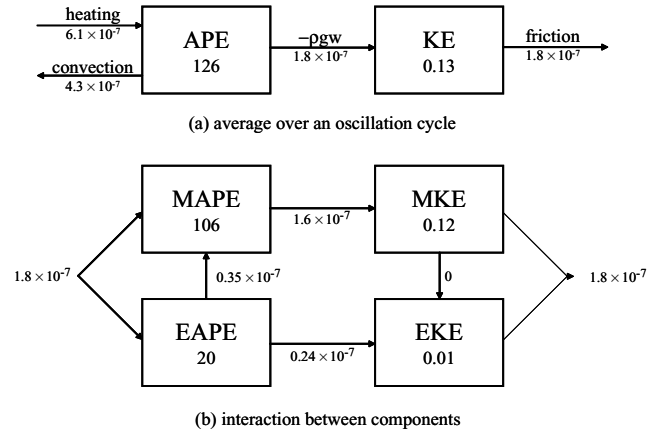


Fig. 10. The global energetics from FLAT. In the upper panel an average over an oscillation cycle, and in the lower panel interaction between the time mean and the fluctuating components are displayed. Unit of energy is kg/ms^2 , and that of conversion rate is kg/ms^3 .

tion is induced by not the mean but anomalous temperature, baroclinic instability may not be the energy source. To illustrate the energy flow, we conducted an energy analysis similar to that described by TD, in which energy analysis was conducted to explain phase relations between various terms. Here, we focus mainly on the time-mean energy budget.

The basin-averaged energy budget averaged over an oscillation cycle from FLAT, following Bryan (1987), is shown in Fig. 10(a). Since there is no wind forcing, the sole energy source is the heating and cooling at the surface, $g\kappa(\hat{\rho}_S - \hat{\rho}_B)/H$, where g is the gravitational constant, κ the vertical diffusivity, ρ_S the surface density and ρ_B the bottom density, the depth of the basin $H = 4$ km, and a hat $\hat{}$ represents a mean over the horizontal area of the basin. About 70% of the energy input by the heating is dissipated by the convection and the remaining 30% is converted into the available potential energy,

$$APE = \langle g\tilde{\rho}^2 / 2\hat{\rho}_z \rangle,$$

and then into the kinetic energy KE by the buoyancy work $-\langle \rho gw \rangle$ to be dissipated by the friction, of which about 95% is due to the lateral friction, as summarized in Fig. 10(a). Here, a bar $\bar{}$ represents a mean over the period of oscillation, a bracket $\langle \rangle$ a basin volume mean as mentioned previously, and $\tilde{\rho} = \rho - \hat{\rho}$. As is well-known, the KE is much smaller than the APE (Bryan, 1987 for example).

Similar to the kinetic energy, the APE is divided into the basin-averaged, time-mean component

$$MAPE = \left\langle g \overline{\hat{\rho}^2} / 2 \hat{\rho}_z \right\rangle,$$

and the fluctuating component,

$$EAPE = \left\langle g \rho'^2 / 2 \hat{\rho}_z \right\rangle, \text{ where } \rho' = \rho - \bar{\rho}.$$

The energy transfer terms (Haidvogel and Beckmann, 1999)

$$MKE \Rightarrow MPE: T_1 = g \langle \bar{w} \bar{\rho} \rangle \quad (5a)$$

$$MAPE \Rightarrow EAPE: T_2 = g \left\langle \overline{\rho' (u' \bar{\rho}_x + v' \bar{\rho}_y)} / \hat{\rho}_z \right\rangle \quad (5b)$$

$$EKE \Rightarrow EAPE: T_3 = g \langle \overline{w' \rho'} \rangle \quad (5c)$$

$$MKE \Rightarrow EKE: T_4 = \left\langle \overline{u' (u' \bar{u}_x + v' \bar{u}_y)} + \overline{v' (u' \bar{v}_x + v' \bar{v}_y)} \right\rangle \quad (5d)$$

are then diagnosed as shown in Fig. 10(b). Since $T_4 = 0$ (it is four orders of magnitude smaller than other terms and considered as zero), and $T_2 < 0$, neither barotropic nor baroclinic instability is responsible for the variability (Haidvogel and Beckmann, 1999). Instead, the variability is maintained by the direct transfer of the *EAPE* to the *EKE* through the buoyancy work (T_3).

Figure 11 shows the temporal structures of the quantities shown in Fig. 10(a). (The frictional dissipation is almost identical to the buoyancy work term and is not included in the figure.) The top-to-bottom stratification ($\hat{\rho}_S - \hat{\rho}_B$)/ H does not change notably. During the warm phase (between Years 10 and 16), the isothermal slope and consequently the *APE* are lower. (The variation of the *APE* follows that of the mean SST at high latitude very closely.) On the other hand, the vertical stratification is stronger, and the convective mixing is harder, resulting in smaller convective dissipation of energy. The opposite occurs during the cold phase (around Year 32).

The temporal variation of the buoyancy work is governed by the sum of $-\langle w' \bar{\rho} \rangle$ and $-\langle \bar{w} \rho' \rangle$. The two quantities show a phase difference (not shown), which TD consider to be a source of the variability and is extensively described. Of course, the time means of both terms are zero. Thus they do not contribute to the net buoyancy work shown in Fig. 10(a), and cannot help us to identify the energy source. Of the two terms, $-\langle w' \bar{\rho} \rangle$ makes the greater contribution and can be used to explain the tendency of the buoyancy work. As explained previously, a

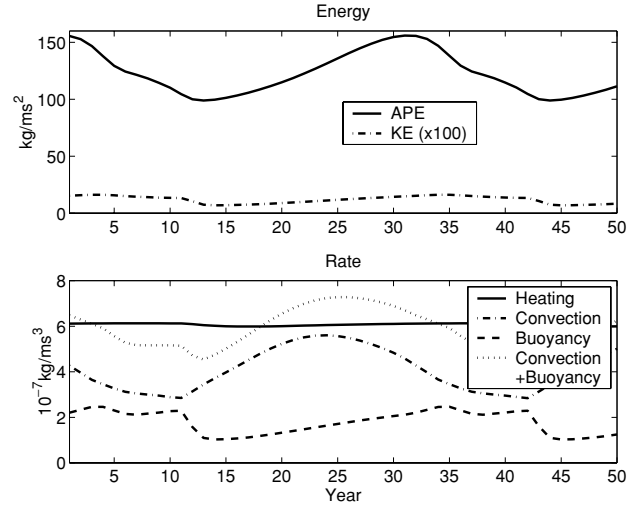


Fig. 11. Time series of the basin volume mean of the *APE*, *KE*, heating, the buoyancy work, and the convective dissipation from FLAT. Note that to compare the *APE* and *KE* in the same plot, $100KE$ is shown in the figure.

cold anomaly along the northern wall enhances an anomalous eastward flow (Year 2 in Fig. 4 for example) and downwelling at the eastern wall (Fig. 6). Therefore, the buoyancy work is greater during the cold phase. Upon switching to the warm phase, the vertical stratification becomes greater and downwelling becomes harder in general. In addition, the negative zonal flow anomaly induces an upwelling anomaly along the eastern and northern walls (Fig. 7). The buoyancy work then decreases rapidly (between Years 11 and 13). As the warm anomaly becomes weaker, the buoyancy work intensifies gradually (between Years 13 and 35). The kinetic energy responds to the buoyancy work instantaneously as well as the frictional dissipation.

The overturning circulation is determined by the vertical velocity. When the downwelling is strongest (weakest), the overturning circulation is strongest (weakest), and the strength of the overturning streamfunction shown in Fig. 9 covaries with the buoyancy work term.

3.4 Effect of bottom topography

In this section we explain the effects of bottom topography on variability shown in Fig. 2, and by previous studies by Winton (1997), Huck *et al.* (2001) and Te Raa *et al.* (2004) by applying results from our energy analysis. The bottom topography modifies the high latitude circulation quite drastically, as discussed in Park and Bryan (2001) or displayed in Fig. 12, in which the mean surface flow patterns from FLAT, BOWL, EAST, NORTH, WEST are compared. In FLAT the eastward zonal flow downwells over the northeastern corner to

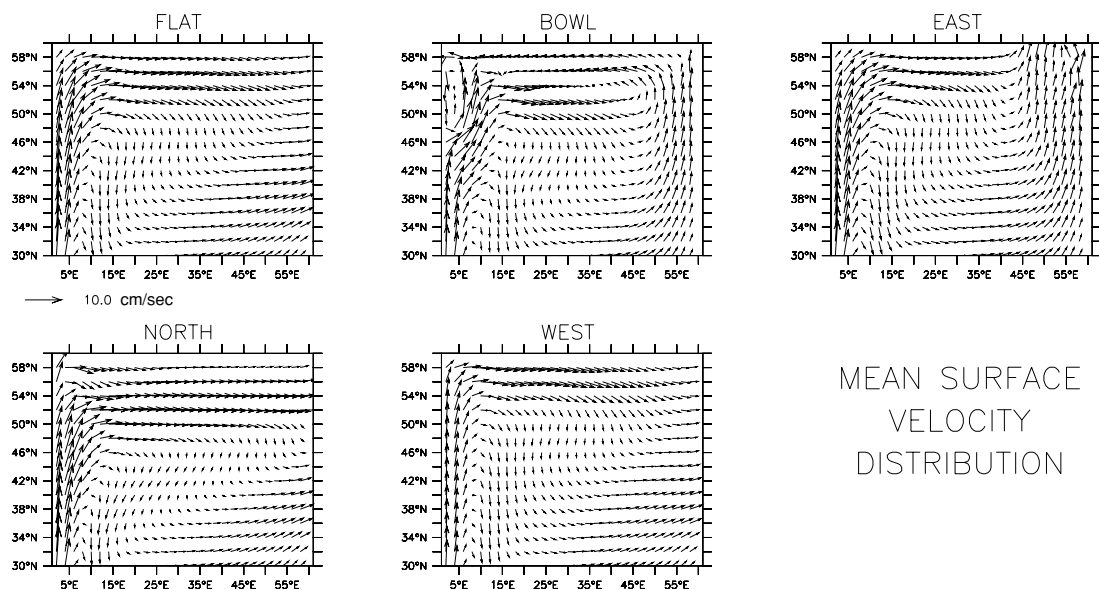


Fig. 12. Mean surface velocity distributions from each case over the northern half of the basin.

become a deep westward zonal flow and no significant flows parallel to the eastern boundary are found. Since the downwelling is strongest at about the 1500 m level and penetrates to the bottom, if a continental shelf is added to the boundaries, which is 200 m deep next to the wall and becomes deeper monotonically to the interior within 12 degrees from the wall, the downwelling is significantly reduced. The zonal flow should then turn to the north to become a flow parallel to the boundary. In BOWL, shelves are added all along the boundaries. The eastward zonal flow found between 50°N and 54°N cannot downwell at the eastern wall because of the shallow topography along the wall. The flow should turn to the north to become a cyclonic boundary current along isobaths that encompass the perimeter of the basin. In NORTH and EAST strong flows parallel to the boundary with a continental shelf are observed. Upon leaving the boundary with the shallow topography, the boundary currents become weaker because there are no isobaths that can guide the flow. In WEST, there is already a dominant flow along the western boundary and no significant change is observed.

In FLAT, the anomalous buoyancy work, $-g\langle w'\rho'\rangle$, which supplies energy for the variability (Fig. 10(b)), is strongest near the boundary where the vertical velocity anomaly is prominent. The vertical velocity anomaly, which attains its maximum at about the 1200 m level (Fig. 6), is found almost over the entire depth. A shelf of 200 m deep cannot allow water to sink to a deeper level, and becomes very effective in reducing the vertical velocity anomaly, and consequently the buoyancy work. Therefore in EAST the conversion of the *EAPE* into *EKE* is reduced to about 30% of that in FLAT and weaker vari-

ability is produced, as listed in Table 2. At the eastern boundary, the vertical velocity anomaly is prominent only over the northern part, but at the northern boundary the velocity anomaly is found all along the boundary (Fig. 7). A shallow shelf along the northern wall is more effective in reducing the vertical velocity anomaly than one along the eastern boundary, so the energy conversion (T_3) and the strength of variability are weaker in NORTH than in EAST. In BOWL, downwelling along both the northern and eastern boundaries is weakened and no variability occurs. The anomalous vertical velocity observed along the western wall is much weaker compared to that along the eastern or the northern wall (Fig. 7), because the western boundary is well stratified due to the western boundary current. A shelf along the western boundary has no have significant effect on the buoyancy work, and the strength of the variability from WEST is not much different from that of FLAT.

3.5 Sensitivity to heat flux pattern

In a double hemispheric rectangular basin with a cyclic channel at the southern end of the basin, Cai *et al.* (1995) and Cai and Chu (1996) investigated the sensitivity of interdecadal thermohaline variability to surface forcing. Upon switching to a heat flux boundary condition, they were not able to observe any variability, if the heat flux diagnosed from a restoring experiment is utilized. When the model was forced with a heat flux obtained by zonally redistributing the diagnosed flux, interdecadal variability was observed. In our experiments, to keep the forcing as simple as possible, we use a zonally uniform heat flux. To investigate whether the vari-

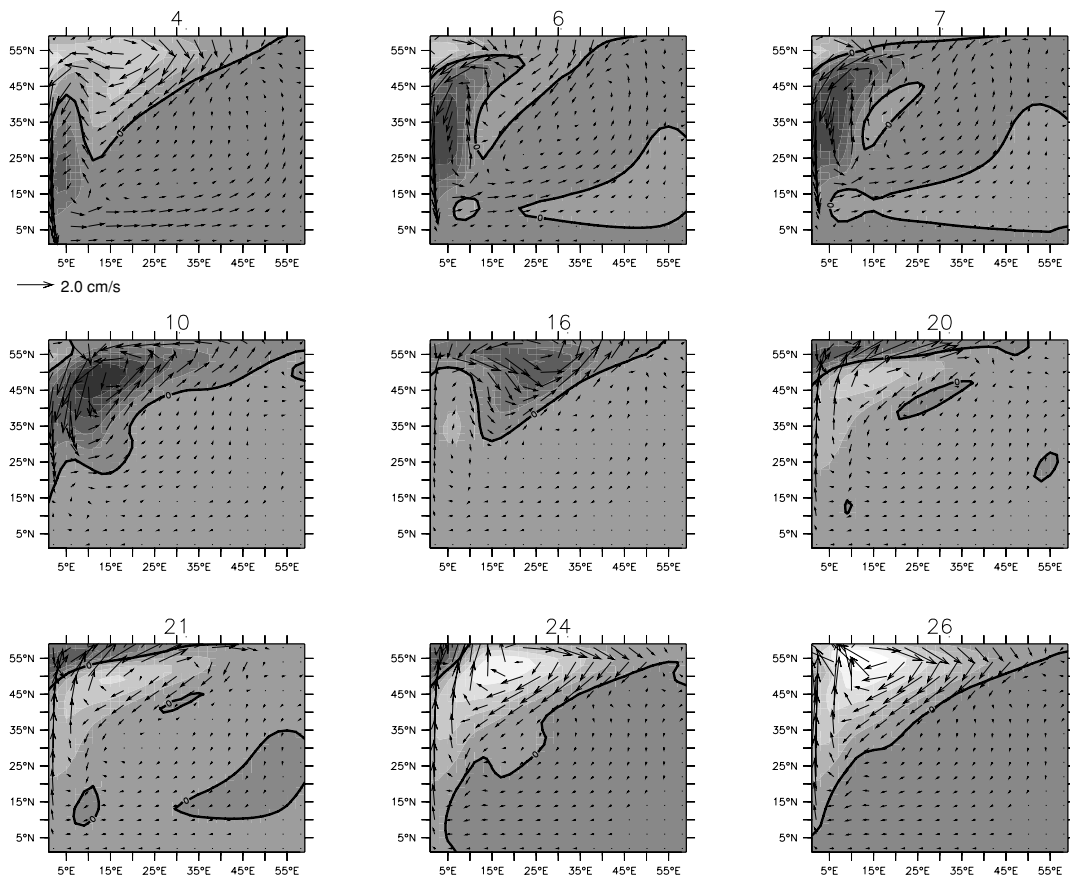


Fig. 13. Evolution of surface temperature (grey scale shading in 0.4°C interval) and velocity anomalies (arrows) from FLUX in which the heat flux shown in Fig. 1(a) is used as the surface heat flux boundary condition. Darker shading means cooler water.

ability we observed is sensitive to the surface heat flux pattern, we conducted another experiment, FLUX, in which the surface heat flux diagnosed from our restoring experiment shown in Fig. 1(a) is used as the surface heat flux boundary condition.

As listed in Table 2, the energetics of FLUX is comparable to that of FLAT. Compared to the FLAT anomalies (Fig. 4), the FLUX anomalies are more prominent over the northwestern corner, but the evolutions of the anomalies in FLUX during an oscillation cycle displayed in Fig. 13 are consistent with the mechanism of variability given in Subsection 3.1. When the warm anomaly is strongest, so that a negative zonal flow is produced, a cold anomaly is formed to the south of the warm anomaly due to the reduction in warm advection (Year 4). The cold anomaly propagates to the northeast (Year 6) to meet the northern wall, and then propagates westward following the northern wall, filling the northern area with cold water (Years 7 and 10). In FLUX the mean flow over the northern part is zonally oriented as in FLAT, but it shows a stronger northward tendency. Thus, in FLAT the anomalies move zonally more or less and encounter the eastern

wall, but in FLUX anomalies move northeastward due to the mean flow and interact with the northern wall instead. Since the anomalies do not cross the basin completely, the period of oscillation in FLUX is shorter than that in FLAT, as shown in Fig. 2. When the northern area is filled with the cold anomaly, the zonal flow becomes stronger and warm advection becomes stronger. A warm anomaly starts to form near the western wall (Year 16) to move northeastward (Year 20). On encountering the northern wall, the anomaly turns cyclonically and moves to the west along the wall (Years 21 and 24). The northern area is filled with warm water, and a cycle of oscillation is completed.

4. Summary and Discussion

The variability of thermohaline circulation is connected to climate variability and many studies have been conducted to understand the structure and governing physics of the variability. To better understand the mechanism of the variability, we have performed idealized numerical experiments with a similar design to earlier studies, such as Winton (1996), and observed interdecadal ther-

mal variability that cyclonically circulates through high latitude areas with about a 32-year period. The main characteristics of the variability from our experiments are similar to those of earlier studies, such as HCW, and Winton (1996). In previous studies, such as HCW and TD, functional relations between globally averaged properties such as overall zonal and meridional overturning circulations have been considered to be the main driving mechanism of such variability. The variability, however, occurs mostly over high latitudes with strong zonal and meridional structures that may disappear if we take the zonal or meridional average. Here we propose a self-sufficient mechanism that does not rely on *a priori* assumptions or relations between zonally or meridionally averaged diagnostic quantities. Our newly proposed mechanism relies on the local interaction among temperature anomalies, horizontal velocity anomalies induced by the temperature anomalies, and the continent blocking the velocity anomalies.

A temperature anomaly located along the northern wall generates a zonal flow anomaly through geostrophy southward of the temperature anomaly. A cold (warm) anomaly along the northern wall produces a positive (negative) zonal flow anomaly that induces a warm (cold) temperature anomaly by enhancing (weakening) warm advection from the western boundary along the path of the zonal flow anomaly. The temperature and the flow anomalies are transported toward the eastern boundary by the mean eastward zonal flow. This eastward propagation of anomaly was not included in TD's explanation. We relate meridional temperature gradient to the formation of a temperature anomaly of an opposite sign, but in TD the former is linked to zonal overturning anomaly. When the positive (negative) zonal flow anomaly that accompanies the warm (cold) temperature anomaly encounters the eastern wall, a downwelling (upwelling) anomaly is produced. To dissipate the vorticity due to this downwelling (upwelling) anomaly, a northward (southward) flow anomaly is generated within a frictional boundary layer next to the eastern wall (Park, 2006). The northward (southward) flow anomaly circulates cyclonically along the perimeter of the basin while enhancing (reducing) warm advection. So does the warm (cold) temperature anomaly carried to the eastern wall by the mean zonal flow while pushing the cold (warm) anomaly that produced the positive (negative) zonal flow anomaly westward and initiating the other half cycle of the variability.

In the mechanism we propose, there are two advective processes that determine the period of the variability. One is the mean zonal flow that is responsible for the eastward propagation of the anomaly. Since the mean zonal flow is 3 cm/s, it takes about 4 to 5 years to move eastwards across the basin. Another time scale is deter-

mined by the flow induced at the eastern wall when the zonal flow anomaly meets the wall. This lies between 1 and 2 cm/s and on the average it would take about 7 years for the warm anomaly to move from the eastern to the western wall. The propagation speed of the cold anomaly is 1/3 to 2/3 of the warm one. If all these values are combined, we get a variability of about 30 years, which is consistent with our experimental results.

One of the key processes in our mechanism is the interaction between the velocity anomalies and the wall. During the interaction, anomalous upwelling or downwelling occurs to modify buoyancy work that releases the available potential energy stored in the stratification. Since buoyancy is the only forcing in the experiments, the available potential energy, of course, is the only energy source. If our explanation is correct, the buoyancy work would be governed by the upwelling or downwelling. Our energy analysis in fact shows that buoyancy work due to anomalous vertical velocity dominates the temporal change of the total buoyancy work. Our energy analysis additionally shows that neither barotropic nor baroclinic instability is responsible for the variability since the energy in the time-mean fields is not converted into that of the fluctuating components.

The sensitivity of the variability to the bottom topography is consistent with our explanation. The vertical velocity anomaly is strongest along the northern wall and the northern part of the eastern wall where the water is well mixed due to convection (Park and Bryan, 2001). The vertical velocity anomaly, the maximum of which occurs at a level deeper than 1000 m, penetrates to the bottom. Thus, if our argument is correct, the variability could be weakened by reducing vertical velocities over those areas with a shelf. As shown in current experiments and earlier studies (Greatbatch *et al.*, 1997; Winton, 1997; Huck *et al.*, 2001; Te Raa *et al.*, 2004), thermal variability is in fact reduced significantly in cases with a shallow shelf along the boundaries. Winton (1997) suggested that bottom topography weakens overturning by weakening the meridional overturning. The meridional overturning estimated on isopycnal coordinate does not show any significant sensitivity to bottom topography (Park and Bryan, 2000), so relating the overturning and variability is not obvious. Our explanation based on local buoyancy work is more plausible.

The anomalous vertical velocity is stronger along the northern wall than the eastern and western ones. Thus, a shallow shelf along the wall is more effective in limiting the buoyancy work and the variability. The western boundary is stratified because of the western boundary current and the anomalous vertical velocity there is weak. A shallow continental shelf added along the boundary does not have a significant effect on the strength of the variability. In a case with shelves all along the boundaries except the

southern one, the anomalous vertical motion is completely prohibited and the variability disappears. Dijkstra (2006) argued that the propagation of the multidecadal mode is based on thermal wind balance, and it is not expected that bottom topography has much influence on the existence of the multidecadal mode. Although the bottom topography may not have much effect on the propagation of anomalies, it modifies the energy conversion and has strong effects on the very existence of the variability.

In our experiments a zonally uniform heat flux is used to keep the forcing as simple as possible. Cai *et al.* (1995) proposed a mismatch between Ocean Dynamics and surface heat flux as a cause of thermal variability. To investigate the validity of our explanation, we conducted an additional experiment in which the surface heat flux diagnosed from the spinup with the restoring condition is used as the surface boundary condition. The shapes of the anomalies are somewhat different from those from the case with the heat flux with no zonal structure. The evolution of the anomalies, however, could be explained in terms of the interactions among the temperature anomalies, the subsequent velocity anomalies induced by the temperature anomalies and their adjustment at the boundary, and proves the robustness of our mechanism.

Acknowledgements

The authors would like to thank the editor and the anonymous reviewers for their comments and suggestions. This research has been funded by KORDI's Research Programs (PM54850 and PP00720). Some of the calculations were performed using the facilities at the Supercomputing Center of KISTI under Strategic Supercomputing Applications Support Programs. The authors wish to acknowledge use of the Ferret program by NOAA's Pacific Marine Environmental Laboratory for some of the analysis and graphics in this paper.

References

- Arzel, O., T. Huck and A. Colin de Verdière (2006): The different nature of the interdecadal variability of the thermohaline circulation under mixed and flux boundary conditions. *J. Phys. Oceanogr.*, **36**, 1703–1717.
- Bryan, F. (1987): Parameter sensitivity of primitive equation ocean general circulation models. *J. Phys. Oceanogr.*, **17**, 970–985.
- Cai, W. J. and P. C. Chu (1996): Ocean climate drift and interdecadal oscillation due to a change in thermal damping. *J. Climate*, **9**, 2821–2833.
- Cai, W. J., R. J. Greatbatch and S. Zhang (1995): Interdecadal variability in an ocean model driven by a small, zonal redistribution of the surface buoyancy flux. *J. Phys. Oceanogr.*, **25**, 1998–2010.
- Clarke, A., J. Church and J. Gould (2001): Ocean processes and climate phenomena. p. 11–30. In *Ocean Circulation and Climate Observing and Modeling the Global Ocean*, Int. Geophys. Ser., Vol. 77, ed. by G. Siedler, J. Church and J. Gould, Elsevier, New York.
- Colin de Verdière, A. and T. Huck (1999): Baroclinic instability: An oceanic wavemaker for interdecadal variability. *J. Phys. Oceanogr.*, **29**, 893–910.
- Delworth, T. L. and R. J. Greatbatch (2000): Multidecadal thermohaline circulation variability driven by atmospheric surface flux forcing. *J. Climate*, **13**, 1481–1495.
- Delworth, T. L. and M. E. Mann (2000): Observed and simulated multidecadal variability in the Northern Hemisphere. *Climate Dyn.*, **16**, 661–676.
- Delworth, T. L., S. Manabe and R. J. Stouffer (1993): Interdecadal variations of the thermohaline circulation in a coupled ocean-atmosphere model. *J. Climate*, **6**, 1993–2011.
- Dijkstra, H. A. (2000): *Nonlinear Physical Oceanography*. Atmos. Oceanogr. Sci. Libr., Vol. 22, Springer, New York, 457 pp.
- Dijkstra, H. A. (2006): The interaction of SST modes in the North Atlantic. *J. Phys. Oceanogr.*, **36**, 286–299.
- Dijkstra, H. A., L. Te Raa, M. Schmeits and J. Gerrits (2006): On the physics of the Atlantic Multidecadal Oscillation. *Ocean Dyn.*, **56**, doi:10.1007/s10236-005-0043-0.
- Greatbatch, R. J. and K. A. Peterson (1996): Interdecadal variability and oceanic thermohaline adjustment. *J. Geophys. Res. [Oceans]*, **101**, 20,467–20,482.
- Greatbatch, R. J. and S. Zhang (1995): An interdecadal oscillation in an idealized ocean basin forced by constant heat flux. *J. Climate*, **8**, 82–91.
- Griffies, S. M. and K. Bryan (1997): Predictability of North Atlantic multidecadal climate variability. *Science*, **275**, 181–184.
- Haidvogel, D. B. and A. Beckmann (1999): *Numerical Ocean Circulation Modeling*. Series on Environmental Science and Management, V. 2, Imperial College Press, London, 318 pp.
- Hasselmann, K. (1976): Stochastic climate model. I: Theory. *Tellus*, **28**, 473–485.
- Huck, T., A. Colin de Verdière and A. J. Weaver (1999): Interdecadal variability of the thermohaline circulation in box-ocean models forced by fixed surface fluxes. *J. Phys. Oceanogr.*, **29**, 865–892.
- Huck, T., G. K. Vallis and A. Colin de Verdière (2001): On the robustness of the interdecadal modes of the thermohaline circulation. *J. Climate*, **14**, 940–963.
- Kravtsov, S. and M. Ghil (2004): Interdecadal variability in a hybrid coupled ocean-atmosphere-sea ice model. *J. Phys. Oceanogr.*, **34**, 1746–1769.
- Kushnir, Y. (1994): Interdecadal variations in North Atlantic sea surface temperature and associated atmospheric conditions. *J. Climate*, **7**, 141–157.
- Park, Y.-G. (2006): Dependence of an eastern boundary current on the horizontal resolution in thermally driven circulations. *J. Geophys. Res. [Oceans]*, **111**, C09005, doi:10.1029/2005JC003362.
- Park, Y.-G. and K. Bryan (2000): Comparison of thermally driven circulations from a depth-coordinate model and an isopycnal-layer model. Part I: Scaling-law sensitivity to vertical diffusivity. *J. Phys. Oceanogr.*, **30**, 590–605.
- Park, Y.-G. and K. Bryan (2001): Comparison of thermally driven circulations from a depth-coordinate model and an isopycnal-layer model. Part II: The difference and struc-

- ture of the circulations. *J. Phys. Oceanogr.*, **31**, 2612–2624.
- Roemmich, D. H. and C. Wunsch (1984): Apparent changes in the climatic state of the deep North Atlantic Ocean. *Nature*, **307**, 447–450.
- Sumata, H. and A. Kubokawa (2001): Numerical study of eastern boundary ventilation and its effects on the thermocline structure. *J. Phys. Oceanogr.*, **31**, 3002–3019.
- Te Raa, L. and H. D. Dijkstra (2002): Instability of the thermohaline ocean circulation on interdecadal timescales. *J. Phys. Oceanogr.*, **32**, 138–160.
- Te Raa, L., J. Gerrits and H. D. Dijkstra (2004): Identification of the mechanism of interdecadal variability in the North Atlantic Ocean. *J. Phys. Oceanogr.*, **34**, 2792–2807.
- Trenberth, K. E. and J. M. Caron (2001): Estimates of meridional atmosphere and ocean heat transports. *J. Climate*, **14**, 3433–3443.
- Trenberth, K. E., J. M. Caron and D. P. Stepaniak (2001): The atmospheric energy budget and implications for surface fluxes and ocean heat transport. *Climate Dyn.*, **17**, 259–276.
- Vonder Haar, T. H. and A. H. Oort (1973): New estimate of annual poleward energy transport by northern hemisphere oceans. *J. Phys. Oceanogr.*, **3**, 169–172.
- Winton, M. (1996): The role of horizontal boundaries in parameter sensitivity and decadal scale variability of coarse-resolution ocean general circulation models. *J. Phys. Oceanogr.*, **26**, 289–304.
- Winton, M. (1997): The damping effect of bottom topography on internal decadal-scale oscillations of the thermohaline circulation. *J. Phys. Oceanogr.*, **27**, 203–208.
- Wunsch, C. (2005): The total meridional heat flux and its oceanic and atmospheric partition. *J. Climate*, **18**, 4374–4380.
- Yin, F. L. and E. S. Sarachik (1995): Interdecadal thermohaline oscillations in a sector ocean general circulation model: Advective and convective processes. *J. Phys. Oceanogr.*, **25**, 2465–2484.